Profile of the U 5*f* magnetization in U/Fe multilayers

S. D. Brown,* L. Bouchenoire,* and P. Thompson*
XMaS, UK-CRG, European Synchrotron Radiation Facility, BP220, F-38043 Grenoble Cedex, France

R. Springell,† A. Mirone, and W. G. Stirling*
European Synchrotron Radiation Facility, BP220, F-38043 Grenoble Cedex, France

A. Beesley and M. F. Thomas
Department of Physics, University of Liverpool, Liverpool L69 7ZE, United Kingdom

R. C. C. Ward and M. R. Wells
Clarendon Laboratory, University of Oxford, Oxford, Oxon OX1 3PU, United Kingdom

S. Langridge
Rutherford Appleton Laboratory, Chilton, Didcot, Oxon OX11 0QX, United Kingdom

S. W. Zochowski
Department of Physics and Astronomy, University College London, London WC1E 6BT, United Kingdom

G. H. Lander
European Commission, JRC, Institute for Transuranium Elements, Postfach 2340, 76125 Karlsruhe, Germany
(Received 18 October 2007; published 18 January 2008)

We have used the x-ray resonant magnetic reflectivity technique to obtain the profile of the induced uranium magnetic moment for selected U/Fe multilayer samples. This study extends the use of x-ray magnetic scattering for induced moment systems to the 5*f* actinide metals. The spatial dependence of the U magnetization shows that the predominant fraction of the polarization is present at the interfacial boundaries, decaying rapidly towards the center of the uranium layer, in good agreement with predictions.

DOI: 10.1103/PhysRevB.77.014427 PACS number(s): 75.70.Cn, 78.70.Ck

I. INTRODUCTION

Magnetic multilayers exhibit a broad range of interesting phenomena, which have both technological and scientific importance.[1] These properties are primarily driven by the electronic interactions at the multilayer interfaces. Our interest lies in the fundamental nature of interactions between the U 5*f* and Fe 3*d* electrons, particularly concerning the magnetism of uranium. We have employed the x-ray resonant magnetic scattering technique in reflection geometry to probe directly the spatial dependence of the U polarization in U/Fe multilayers.

Theoretical predictions have been made regarding the polarization of uranium in U/Fe multilayer systems, based on both scalar and fully relativistic calculations.[2] The approach adopted an exchange correlation potential treated in the generalized gradient approximation, which reproduced earlier theoretical predictions for the magnetism of the surface of alpha uranium.[3] A model U(001)/Fe(110) supercell structure was proposed with lattice constants taken as the average between those for uranium and iron. The calculations revealed the importance of U-Fe electronic hybridization and predicted a spin moment on the uranium site of $0.92\mu_B$, significantly larger and aligned opposite to that of the orbital moment, $0.16\mu_B$. The total uranium moment was predicted to align antiparallel to the Fe moments and to decrease rapidly within just two atomic layers.

Since the first experimental evidence for x-ray magnetic scattering,[4] advances in x-ray sources and development of new materials have lead to a surge of scientific activity in this field. This has been aided by the discovery of large resonant enhancements of the magnetic scattering at the $L_{2,3}$ edges of the rare earth metals[5] and the $M_{4,5}$ edges of the actinides.[6,7] In multicomponent systems, such as magnetic multilayers, resonant enhancements of the scattering factor can dramatically improve the chemical contrast between elements. Moreover, it is possible to detect strong magnetic dichroism at these resonant absorption edges with the employment of polarized x rays. X-ray resonant magnetic reflectivity (XRMR) combines the benefits of magnetic dichroism with structural information from the charge scattering so that it is possible to determine the spatial profile of the magnetization within the layers. It is a technique ideally suited to the investigation of the magnetism of uranium in U/Fe multilayers. The use of XRMR to investigate buried interfaces in magnetic nanostructures is well documented, certainly for the case of soft x rays,[8] but has been less exploited in the hard x-ray regime. At these energies, it is most often the *L* edges of the rare-earth elements which are of interest,[9] but some progress has been made in understanding the induced moment in 5*d* transition metal systems also.[10]

Preliminary measurements at the U M_4 edge have reported an induced magnetic moment on the U site[11] and later, the separation of spin and orbital components of this moment, using x-ray magnetic circular dichroism (XMCD).[12] The total magnetic moments in this case are small ($\sim 0.1\mu_B$). However, the element selectivity and brightness

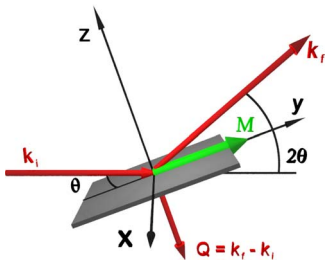

FIG. 1. (Color online) Schematic diagram of the longitudinal geometry used in the XRMR measurements. $\mathbf{k_i}$ and $\mathbf{k_f}$ are the wave vectors of the incoming and outgoing circularly polarized x rays, respectively. **M** is the magnetization of the sample. The applied field **H** is parallel to **M**.

of x rays at a synchrotron source, coupled with the large resonances of the U *M* edges, allow the moments to be easily detected. The XMCD technique provides only an average of the U magnetization for the whole multilayer and is not sensitive to the distribution of the $5f$ polarization within the layer. The spatial dependence of the induced U moment, determined by XRMR, provides a unique insight into the extent of the U $5f$ and Fe $3d$ interactions.

II. X-RAY RESONANT MAGNETIC REFLECTIVITY

X-ray reflectivity measurements have become standard practise for determining the structure of multilayers. Most commonly, a single wavelength measurement is used and a calculation of the reflected intensity, based on Parratt's recursive method,[13] is employed to model the layer thickness and roughness parameters. However, in order to determine the profile of the magnetization of a layer, particularly one whose polarization is strongly thickness dependent, it is important to determine more precisely the interfacial structure. This can be achieved by varying the electronic contrast of the respective elements, measuring the scattered intensity as a function of energy through an absorption edge of one of the constituent materials, in this case the M_4 edge of uranium.

Once the multilayer structure has been determined, it is possible to measure the **Q**-dependent magnetic scattering. By employing circularly polarized synchrotron radiation and applying a magnetic field at the sample position, the magnetic signal is detected as the difference in intensity of the elastic scattering when either the helicity of the incoming x rays or the magnetic field direction is reversed. The experimental geometry is shown in Fig. 1.

The atomic scattering factor, $F(E)$, can be written in terms of a combination of charge, $F_c(E)$, and magnetic, $F_m(E)$, structure factors.[14]

$$F(E) = (\hat{\varepsilon}_\mathbf{f} \cdot \hat{\varepsilon}_\mathbf{i}) F_c(E) - i(\hat{\varepsilon}_\mathbf{f} \times \hat{\varepsilon}_\mathbf{i}) F_m(E), \tag{1}$$

where $\hat{\varepsilon}_\mathbf{i}$ and $\hat{\varepsilon}_\mathbf{f}$ are the unit polarization vectors of the incident and scattered x rays, respectively. The charge structure factor can be written as a summation over all the atoms in the multilayer,

$$F_c = \sum [f_0 + f_c'(E) + i f_c''(E)] e^{i\mathbf{Q}\cdot\mathbf{r}}, \tag{2}$$

where f_0 is the tabulated atomic form factor[15] and $f_c'(E)$ and $f_c''(E)$ are the real and imaginary parts of the complex resonant anomalous scattering factor, respectively. The resonant magnetic structure factor can be written in a similar way, as a summation over the resonating magnetic atoms,

$$F_m = \sum \hat{\mathbf{m}} [f_m'(E) + i f_m''(E)] e^{i\mathbf{Q}\cdot\mathbf{r}}. \tag{3}$$

Here, $f_m'(E)$ and $f_m''(E)$ are the real and imaginary parts of the resonant magnetic scattering factor, respectively, and $\hat{\mathbf{m}}$ is the unit vector along the quantization axis parallel to the sample magnetization **M**. The U M_4 absorption edge represents the excitation of electrons from the $3d_{3/2}$ to the $5f_{5/2}$ states, where electric dipole transitions provide the strongest contributions to the magnetic scattering.[16] For dipole transitions, the resonant magnetic scattering factors can be represented as

$$f_m'(E) + i f_m''(E) = \left(\frac{3}{4kr_e}\right)[F_{11}(E) - F_{1-1}(E)], \tag{4}$$

where F_{LM} are determined by atomic properties and are related to the strength of the resonance,[17] r_e is the classical electron radius, and k is the wave vector.

The intensities observed in elastic scattering are related to the square of the atomic scattering factor, which on inspection of Eq. (1) yields cross terms that represent the resonant magnetic-charge interference scattering.

$$\sum |F^+|^2 - \sum |F^-|^2 = -2(\hat{\mathbf{k}} + \hat{\mathbf{k}}' \cos 2\theta) \cdot (F_c' F_m' + F_c'' F_m'') \tag{5}$$

$$= I^+ - I^-. \tag{6}$$

The magnetic-charge interference can be accessed either by reversing the helicity of the incoming photons or by reversing the magnetic field. Conventionally, "+" represents right circularly polarized x rays and "−" represents left. In our case, we held the polarization constant and reversed the magnetic field. The geometric term in Eq. (5) indicates that the magnetic-charge interference scattering is only sensitive to the component of the magnetization within the scattering plane; hence, the magnetic field was applied along the direction defined by the sample plane and the scattering plane (see Fig. 1).

The scattered intensity was modeled by adapting Parratt's recursion formula[13] for nonmagnetic specular reflectivity from a multilayer. The complex amplitudes of the electric fields of the transmitted and reflected x rays of both magnetic field states were included in the calculations. In the frame of reference of the incoming circularly polarized x-ray beam, the x rays experience different refractive indices for each of the magnetic field directions, $n^\pm = 1 - \delta^\pm + i\beta^\pm$, with

$$\delta^\pm = \left(\frac{2\pi n_0 r_e}{k^2}\right)[f_0 + f_c'(E) \mp f_m'(E) \cos\theta \cos\phi], \tag{7}$$

$$\beta^{\pm} = \left(\frac{2\pi n_0 r_e}{k^2}\right)[f_c''(E) \mp f_m''(E)\cos\theta\cos\phi], \tag{8}$$

where n_0 is the number of atoms per unit volume. The imaginary parts of the charge and magnetic scattering factors are then modeled as a function of energy and a Kramers-Kronig transformation used to relate the real and imaginary parts of the respective scattering factors.

Commonly, the optical parameters are well known, such as for the transition metal L edges, and only a token number of energies need be sampled to describe the energy dependence of the scattered intensity. Another approach is to measure the fluorescence and calculate the XMCD, where the XMCD absorption coefficient is related to the imaginary part of the magnetic scattering factor,

$$\mu_m(E) = -\left(\frac{8\pi n_0 r_e}{k}\right)(\hat{\mathbf{k}}\cdot\hat{\mathbf{m}})f_m''(E). \tag{9}$$

However, significant self-absorption effects can be present in fluorescence measurements.[18] The corrections for these effects then presuppose a knowledge of the structure. In our case, the optical constants are not well known and the resonance at the U M_4 edge is large. Also, previous measurements on the U/Fe system[19–21] have indicated that the structure of the U/Fe multilayer interfaces cannot be modeled simply. In this investigation, we have used a double Lorentzian squared line shape to model the imaginary part of the scattering factor and an arctan function to model the nonresonant photoelectric absorption. A total of 17 energies were used to precisely track the scattered intensity as a function of energy.

The layer was divided into slices along the z direction, approximately one atomic plane in thickness (~2.5 Å). The interfacial structure was then modeled by varying the relative densities of the uranium and iron to give a profile of both the U and Fe densities through the multilayer. The calculation of the charge scattering was fitted to the experimental data simultaneously for two different multilayers at all energies. Several parameters were held constant from sample to sample. An important simplification included using identical interfacial regions for each bilayer for each sample.

In order to determine a profile of the induced U magnetization, a coefficient was applied to the magnetic scattering factors for each slice of the bilayer that contained some uranium density. The coefficients are proportional to the magnetic moment per uranium atom; hence, by fitting these values to the magnetic-charge interference scattering, it is possible to model the spatial dependence of the induced U 5*f* polarization along the growth direction.

III. EXPERIMENTAL DETAILS

The samples were prepared in the Clarendon Laboratory, University of Oxford, by dc magnetron sputtering in a UHV load-locked growth chamber, operating at a base pressure of 5×10^{-10} mbar. The multilayers were grown on 50 Å thick niobium buffer layers deposited onto single-crystal sapphire plates. The multilayers were sputtered at a growth rate of ~1 Å/s in an argon atmosphere of 5×10^{-3} mbar. The samples were protected from oxidation by a 50 Å Nb capping layer. The structural and bulk magnetic properties have been reported previously.[21,22]

The XRMR measurements were carried out at the XMaS beamline (BM28) at the ESRF in Grenoble. This beamline is situated on a bending magnet section of the synchrotron, where the optics and experimental hutch setup have been designed for the study of x-ray magnetic scattering and the photon flux has been optimized at energies in the vicinity of the U M edges. A complete description of the beamline optics and experimental capabilities is given by Brown *et al.*[23] The sample views the x-ray beam on orbit, so that the incident flux is linearly polarized. An ~70% rate of circular polarization was achieved, by employing a diamond (111), quarter-wave phase plate.[24] This polarization was verified at the beginning of the experiments. In order to preserve as much flux as possible, necessary at the relatively low energies of the uranium M edges, the flight paths of the incident and scattered x rays were under vacuum.

The samples, on copper mounts, were attached to a magnet assembly, consisting of water-cooled pole pieces, generating an applied magnetic field of 0.1 T. This field was large enough to saturate the iron moments, but small enough to be reversed rapidly. The pole pieces were arranged so that they could provide a field aligned parallel to the scattering plane. The magnet was fixed on a precision sample mount on an 11 circle Huber diffractometer and a Bicron detector was mounted on the 2θ arm. All experiments were performed at room temperature, as the previous studies showed a significant dichroic signal up to 300 K.[12]

The measurements were carried out on two U/Fe samples, SN71, $[U_9/Fe_{34}]_{30}$ and SN76, $[U_{27}/Fe_{57}]_{20}$ (element subscripts give the layer thickness in angstroms and the bracket subscript the number of bilayer repeats), whose nominal layer thicknesses were determined by x-ray reflectivity.[21] XRMR measurements were made across the U M_4 edge (3728 eV) for circularly polarized x rays in an applied field of 0.1 T. Data were collected for 17 energies spanning 20 eV below the M_4 edge to 20 eV above, providing a mesh of the x-ray reflectivity and magnetic-charge interference scattering (defined as I^+-I^-) as a function of **Q** and energy.

IV. RESULTS

Figure 2 shows the experimental x-ray resonant reflectivity data and calculated intensities for sample SN71. The model reproduces well the fine detail contained between the Bragg peaks and the changes in the reflectivity with energy. A particular feature is the broadening of the Bragg peaks at the resonant energy. Figure 3 shows the (a) real and (b) imaginary parts of the resonant scattering factor. The imaginary part was determined from the model described in Sec. II and the real part was taken as its Kramers-Kronig transform, both shown in electron units. The insert of Fig. 3(b) shows a comparison of the self-absorption corrected fluorescence data[12] with the imaginary part of the resonant scattering factor.

The magnetic-charge interference scattering (I^+-I^-) was calculated separately for each sample. Real and imaginary

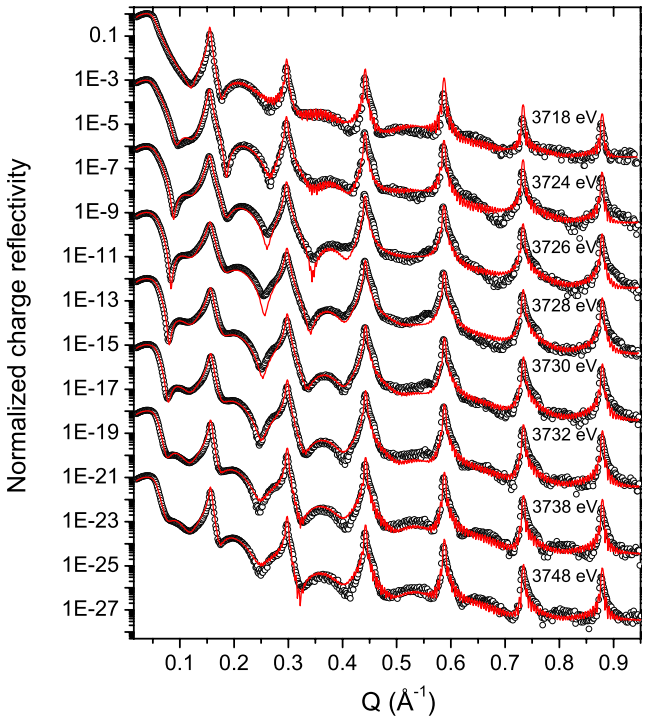

FIG. 2. (Color online) Energy variation of the charge reflectivity in the vicinity of the U M_4 edge for sample SN71. The experimental data are shown as the open black circles and the calculated reflectivity is represented by the solid red line. The spectra have been scaled by factors of 10^{-3} between each energy.

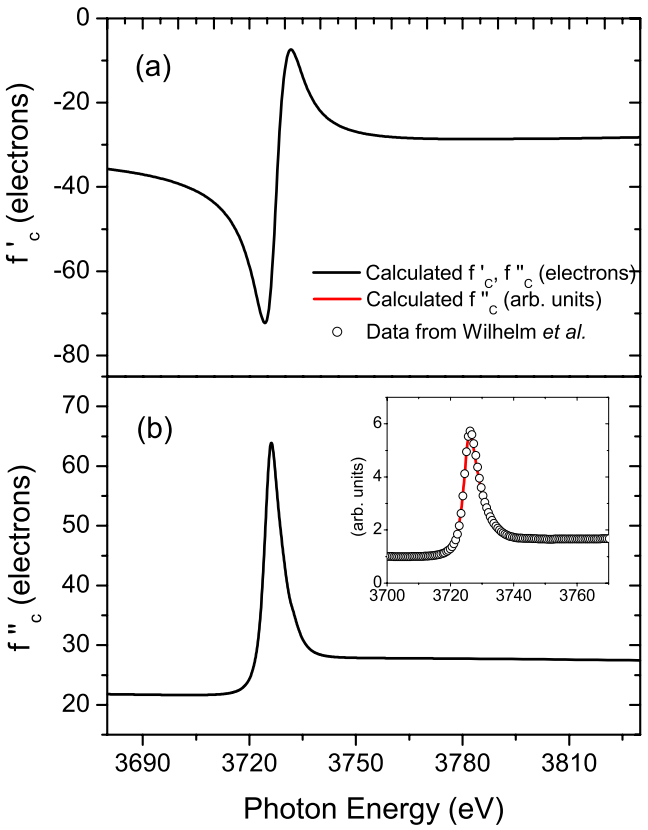

FIG. 3. (Color online) The (a) real and (b) imaginary parts of the resonant charge scattering factor are shown in electron units for sample SN71. The imaginary part is determined from the calculations of the charge reflectivity and the real part is its Kramers-Kronig transform. The insert of (b) is a comparison of the modeled imaginary scattering factor and the fluorescence, reported previously (Ref. 12).

magnetic scattering factors were modeled for each sample. Figure 4 shows the magnetic difference across the first four Bragg peaks in the vicinity of the U M_4 edge for sample SN71, compared to the fitted calculation. Higher order Bragg peaks did not yield a measurable magnetic effect. The experimental data and the calculated intensities have been scaled by the theoretical **Q** dependence of the reflected intensity.

The imaginary part of the magnetic scattering factor used to model the magnetic-charge interference scattering for sample SN71 is shown in Fig. 5(b) and the real part in Fig. 5(a) is its Kramers-Kronig transform. The insert of Fig. 5(b) shows a comparison between the XMCD signal determined from the imaginary part of the magnetic scattering factor (normalized to the imaginary part of the charge scattering factor) and XMCD data (normalized to the fluorescence) measured on the same sample at room temperature and in an applied field of 1 T.[12]

V. DISCUSSION

The agreement between calculated and experimental data is good for both structural and magnetic data. The scattering factors of Fig. 3, determined from the fitted calculations of the charge scattering, are similar in shape and magnitude to those measured across the U M_4 edge in other uranium systems.[25] Good agreement between the fluorescence measurements, corrected for self absorption effects,[12] and the imaginary part of the resonant scattering factor, shown in Fig. 3(b), may be attributed to the large number of energies sampled. This is also supported by the comparison of the XMCD signals shown in the insert of Fig. 5(b).

The relative densities of the uranium and iron within a bilayer are shown in panels (a) and (c) of Fig. 6 for samples SN71 and SN76, respectively. The density profiles show extended regions on either side of the central iron and uranium layers, which consist of a mixture of iron and uranium atoms. Error bars in these figures are estimated at 0.1 along the ordinate axis. The results are consistent with the models proposed in earlier studies, using the Mössbauer technique[20] and suggests that the nonmagnetic "dead" layer[22] could be a result of the alloying of the Fe atoms in the interfaces, labeled as amorphous Fe in Fig. 6. These alloy-type regions account for effects of interfacial roughness and interdiffusion that can dramatically alter the profile of the magnetization.[26]

The magnetic-charge interference scattering was calculated by assigning a magnetization to each slice of the bilayer containing uranium. The calculations were fitted to the experimental data without restrictions on the shape or symmetry of the profile. The resultant profiles of the induced magnetization within the uranium component of the multilayers are shown in panels (b) and (d) of Fig. 6 and are

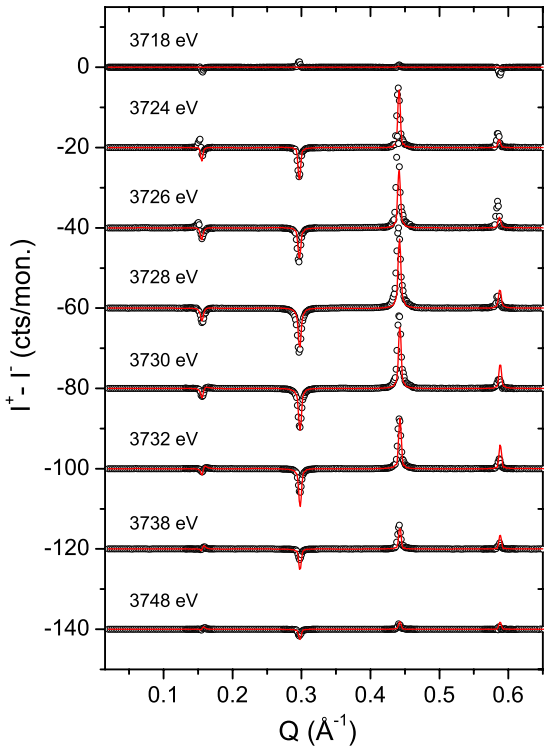

FIG. 4. (Color online) The magnetic-charge interference scattering as a function of energy across the U M_4 edge for sample SN71. The data are shown as the open black circles and the fitted calculation is represented by the solid red line, both are scaled by a $\mathbf{Q}^4$ factor. The results presented for each energy have been offset by 20 cts/mon for clarity, where cts/mon indicates the intensity normalized to the incident beam.

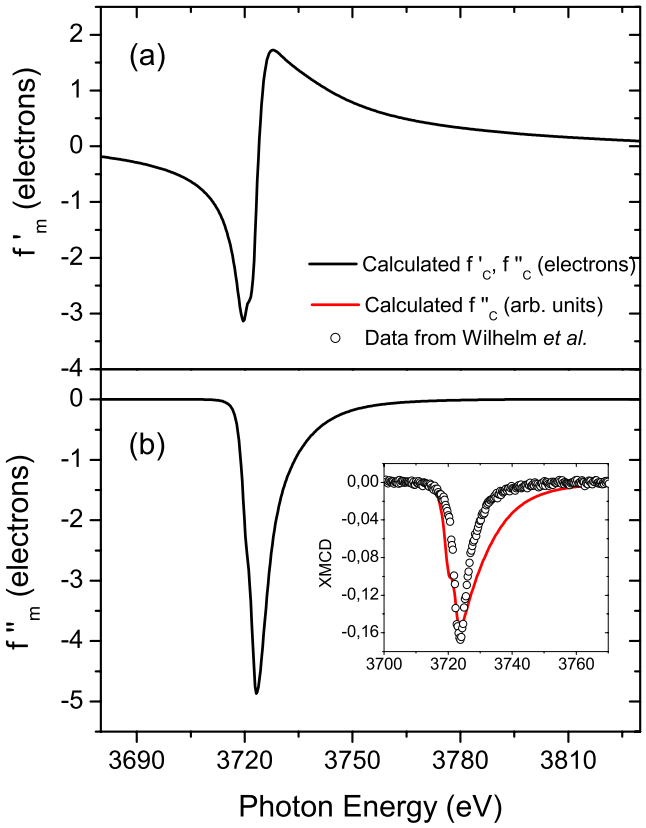

FIG. 5. (Color online) The (a) real and (b) imaginary parts of the resonant magnetic scattering factor for sample SN71. The imaginary part is determined from the calculations of the charge-magnetic interference scattering and the real part is its Kramers-Kronig transform. The insert of (b) is a comparison of the XMCD signals determined by this model and measurements made at room temperature in a field of 1 T by Wilhelm *et al.* (Ref. 12).

scaled to the relative densities of uranium in each slice. The profile has then been normalized to the total magnetic moment, as determined from XMCD measurements,[12] to give the induced uranium magnetization in units of μ_B/U. It is clear that the polarization occurs mainly when the uranium atoms are close to the central iron layers, which contain the magnetic bcc component. Furthermore, the magnetization of the uranium falls off rapidly away from the central iron layers and is in the same direction at each side of the interface. Small differences between this profile and that constructed from the XMCD investigation (Fig. 9 of Ref. 12) are due to different resolution with respect to the widths of the slices, and in addition, due to assumptions of sharp U/Fe interfaces and a symmetric magnetization profile. The XRMR study reported here shows that such assumptions are incorrect; however, the general conclusions of Ref. 12 remain valid.

Theoretical studies of the polarization of uranium in U/Fe multilayers used a model system, which consisted of a sharp interface region and a lattice-matched superstructure.[2] A moment of about $1\mu_B$ was predicted, but was found to be considerably smaller ($\sim 0.1\mu_B$) in XMCD studies.[12] This can be attributed to differences between the idealized model calculation and the real multilayers. The spatial dependence of the induced magnetic moment is predicted to fall away very quickly from the maximum value, so that within two atomic planes (~ 5 Å), it is almost zero. In this respect, the calculations and experimental data are in good agreement.

VI. CONCLUSIONS

Energy dependent x-ray resonant reflectivity at the U M_4 edge has been used to determine the detailed structure of U/Fe multilayers. Interfacial regions are present, containing a uranium-iron alloy. The fitted charge scattering factors shown in Fig. 3 are similar to those found in other uranium systems[25] and are in close agreement with fluorescence data corrected for self-absorption.[12]

The magnetic-charge interference scattering has been used to determine the profile of the uranium magnetization. Agreement between calculation and experiment could be achieved only with the introduction of extended interdiffused regions at the interfacial boundaries. The U polarization is predominantly at the low uranium concentration end of the interface, in close proximity to the bcc iron and decays rapidly as a function of depth toward the center of the uranium layer. This is in qualitative agreement with theoretical calculations,[2] emphasizing the importance of the $3d$-$5f$ hybridization for the induced magnetization of uranium in U/Fe multilayers.

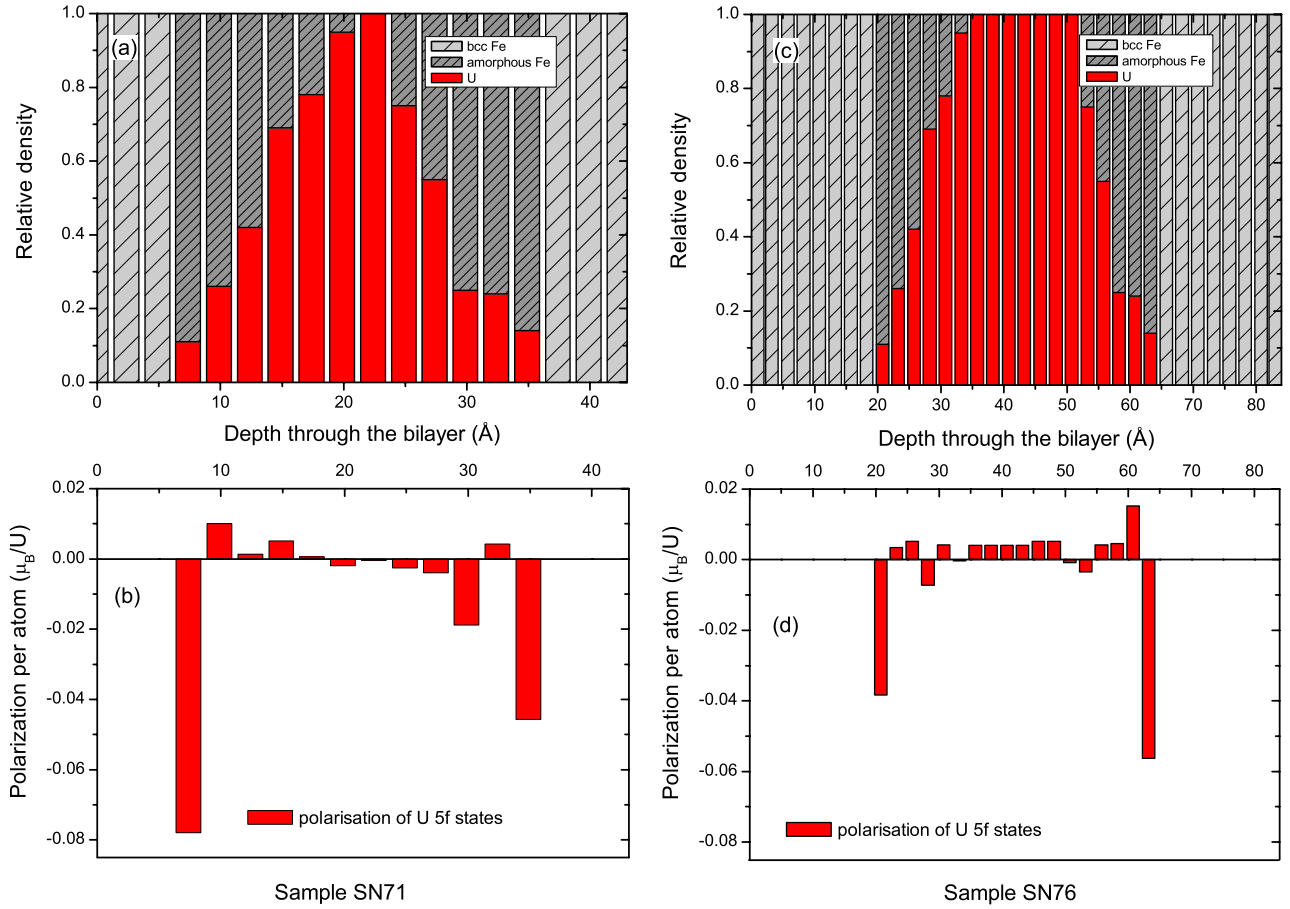

FIG. 6. (Color online) Profiles of the relative uranium and iron densities as a function of bilayer depth are shown in panels (a) and (c) of Fig. 6 for samples SN71 and SN76, respectively. The errors in the relative density are estimated as ± 0.1. Panels (b) and (d) present the profiles of the uranium polarization, given in units of μ_B/U determined from XMCD measurements (Ref. 12). The error bars are estimated as $\pm 0.02 \mu_B$/U. We note that the dominant negative sign of the polarization is an assumption, based on XMCD (Ref. 12) and theory (Refs. 2 and 3).

ACKNOWLEDGMENTS

R.S. acknowledges the receipt of an EPSRC research studentship. We are grateful to the EPSRC in the UK for funding the XMaS beamline facility through the universities of Liverpool and Warwick.

*Also at Department of Physics, University of Liverpool, Liverpool L69 7ZE, United Kingdom.
†Also at Department of Physics and Astronomy, University College London, London WC1E 6BT, United Kingdom.

[1] J. A. C. Bland and B. Heinrich, *Ultrathin Magnetic Structures I: An Introduction to the Electronic, Magnetic and Structural Properties* (Springer-Verlag, Berlin, 1994).
[2] A. Laref, E. Şaşioğlu, and L. M. Sandratskii, J. Phys.: Condens. Matter **18**, 4177 (2006).
[3] N. Stojić, J. W. Davenport, M. Komelj, and J. Glimm, Phys. Rev. B **68**, 094407 (2003).
[4] F. de Bergevin and M. Brunel, Phys. Lett. **39A**, 141 (1972).
[5] D. Gibbs, D. R. Harshman, E. D. Isaacs, D. B. McWhan, D. Mills, and C. Vettier, Phys. Rev. Lett. **61**, 1241 (1988).
[6] E. D. Isaacs, D. B. McWhan, C. Peters, G. E. Ice, D. P. Siddons, J. B. Hastings, C. Vettier, and O. Vogt, Phys. Rev. Lett. **62**, 1671 (1989).
[7] C. C. Tang, W. G. Stirling, G. H. Lander, D. Gibbs, W. Herzog, P. Carra, B. T. Thole, K. Mattenberger, and O. Vogt, Phys. Rev. B **46**, 5287 (1992).
[8] J. Grabis, A. Bergmann, A. Nefedov, K. Westerholt, and H. Zabel, Phys. Rev. B **72**, 024438 (2005).
[9] L. Sève, N. Jaouen, J. M. Tonnerre, D. Raoux, F. Bartolomé, M. Arend, W. Felsch, A. Rogalev, J. Goulon, C. Gautier *et al.*, Phys. Rev. B **60**, 9662 (1999).
[10] N. Jaouen, G. van der Laan, T. K. Johal, F. Wilhelm, A. Rogalev, S. Mylonas, and L. Ortega, Phys. Rev. B **70**, 094417 (2004).
[11] S. D. Brown, A. Beesley, A. Herring, D. Mannix, M. F. Thomas, P. Thompson, L. Bouchenoire, S. Langridge, G. H. Lander, W. G. Stirling *et al.*, J. Appl. Phys. **93**, 6519 (2003).

[12] F. Wilhelm, N. Jaouen, A. Rogalev, W. G. Stirling, R. Springell, S. Zochowski, A. M. Beesley, S. D. Brown, M. F. Thomas, G. H. Lander *et al.*, Phys. Rev. B **76**, 024425 (2007).
[13] L. G. Parratt, Phys. Rev. **95**, 359 (1954).
[14] J. P. Hannon, G. T. Trammell, M. Blume, and D. Gibbs, Phys. Rev. Lett. **61**, 1245 (1988).
[15] B. L. Henke, E. M. Gullikson, and J. C. Davis, At. Data Nucl. Data Tables **54**, 181 1993.
[16] G. van der Laan and B. T. Thole, Phys. Rev. B **53**, 14458 (1996).
[17] J. P. Hill and D. F. McMorrow, Acta Crystallogr. **52**, 236 (1996).
[18] P. Pfalzer, J.-P. Urbach, M. Klemm, S. Horn, M. L. denBoer, A. I. Frenkel, and J. P. Kirkland, Phys. Rev. B **60**, 9335 (1999).
[19] A. M. Beesley, M. F. Thomas, A. D. F. Herring, R. C. C. Ward, M. R. Wells, S. Langridge, S. D. Brown, S. W. Zochowski, L. Bouchenoire, W. G. Stirling *et al.*, J. Phys.: Condens. Matter **16**, 8491 (2004).
[20] A. M. Beesley, S. W. Zochowski, M. F. Thomas, A. D. F. Herring, S. Langridge, S. D. Brown, R. C. C. Ward, M. R. Wells, R. Springell, W. G. Stirling *et al.*, J. Phys.: Condens. Matter **16**, 8507 (2004).
[21] R. Springell, S. W. Zochowski, R. C. C. Ward, M. R. Wells, S. D. Brown, L. Bouchenoire, F. Wilhelm, S. Langridge, W. G. Stirling, and G. H. Lander, arXiv:0704.3947 (unpublished).
[22] R. Springell, S. W. Zochowski, R. C. C. Ward, M. R. Wells, S. D. Brown, L. Bouchenoire, F. Wilhelm, S. Langridge, W. G. Stirling, and G. H. Lander, arXiv:0704.3970 (unpublished).
[23] S. D. Brown, L. Bouchenoire, D. B. J. Kervin, D. Laundy, M. J. Longfield, D. Mannix, D. F. Paul, A. Stunault, P. Thompson, M. J. Cooper *et al.*, J. Synchrotron Radiat. **8**, 1172 (2001).
[24] L. Bouchenoire, S. D. Brown, P. Thompson, J. A. Duffy, J. W. Taylor, and M. J. Cooper, J. Synchrotron Radiat. **10**, 172 (2003).
[25] G. M. Watson, D. Gibbs, G. H. Lander, B. D. Gaulin, L. E. Berman, H. Matzke, and W. Ellis, Phys. Rev. B **61**, 8966 (2000).
[26] O. Sipr, J. Minár, J. Vackář, and H. Ebert, Phys. Rev. B **75**, 134422 (2007).